Redox-Coupled Crystal Structural Changes in Bovine Heart Cytochrome c Oxidase

Shinya Yoshikawa,* Kyoko Shinzawa-Itoh, Ryosuke Nakashima, Rieko Yaono, Eiki Yamashita, Noriko Inoue, Min Yao, Ming Jie Fei, Clare Peters Libeu, Tsunehiro Mizushima, Hiroshi Yamaguchi, Takashi Tomizaki, Tomitake Tsukihara

Crystal structures of bovine heart cytochrome c oxidase in the fully oxidized, fully reduced, azide-bound, and carbon monoxide–bound states were determined at 2.30, 2.35, 2.9, and 2.8 angstrom resolution, respectively. An aspartate residue apart from the O_2 reduction site exchanges its effective accessibility to the matrix aqueous phase for one to the cytosolic phase concomitantly with a significant decrease in the pK of its carboxyl group, on reduction of the metal sites. The movement indicates the aspartate as the proton pumping site. A tyrosine acidified by a covalently linked imidazole nitrogen is a possible proton donor for the O_2 reduction by the enzyme.

Cytochrome c oxidase, a key enzyme in cell respiration, catalyzes the reduction of O_2 to water at the site involving heme a_3 and Cu_B (heme a_3–Cu_B site hereafter) by means of protons extracted from the matrix side of the inner mitochondrial membrane and electrons from cytochrome c, in a reaction that is coupled with proton pumping (*1*). The crystal structures of a eukaryotic and a prokaryotic cytochrome c oxidase previously reported at 2.8 Å resolution ushered in a new era for cytochrome c oxidase research (*2*–*4*).

For the proton pumping function of cytochrome c oxidase driven by the O_2 reduction, an acidic group in the protein must be accessible only to one of the two bulk water phases on both sides of the mitochondrial membrane in a certain oxidation state of the enzyme, and the accessible side must be switched to the other side by a change in the oxidation state, concomitantly with a significant change in the pK of the acidic group. The changes in accessibility and pK can be induced by very small conformational changes in the protein. Thus, careful comparison of the crystal structure in various oxidation and ligand-binding states at high resolution is indispensable for understanding the mechanism of proton pumping by this enzyme.

Crystallization conditions have been improved to provide crystals that diffract x-rays up to 1.9 Å resolution (*5*). Crystals of the fully oxidized, fully reduced, fully reduced CO-bound, and fully oxidized azide-bound forms were prepared from the crystals of the fully oxidized form (*5*). Intensity data and phase determinations of these states are summarized in Table 1. The crystal structures were refined with the program XPLOR (*6*). The statistics of the structural refinement of these crystals are given in Table 2.

Structure of the heart a_3–Cu_B site. The electron density for His^{240} and Tyr^{244} of subunit I given as an $(F_o - F_c)$ difference Fourier map (*7*) at 2.3 Å resolution indicates the presence of a covalent bond between $N\varepsilon_2$ of His^{240} imidazole group and $C\varepsilon_2$ of Tyr^{244} phenol group (Fig. 1A). This covalent linkage is also apparent in the electron density distribution of the fully reduced enzyme at 2.35 Å resolution and is consistent with the electron density maps of the fully reduced CO-bound form and the fully oxidized azide-bound form. The covalent linkage has been proposed also for the fully oxidized *Paracoccus* cytochrome c oxidase at 2.7 Å resolution (*8*). The covalent linkage suggests that the pK of the TyrOH is significantly lower than that of free TyrOH. Thus, a significant fraction of OH group of Tyr^{244} may be in the deprotonated form even in the physiological pH.

The $(F_o - F_c)$ difference Fourier map (*7*) of the oxidized form (Fig. 1A) shows also a residual density between heme a_3 iron (Fe_{a3}) and Cu_B. The refined model for the residual electron density in the heme a_3–Cu_B site of the fully oxidized form (Fig. 1A and Table 3) is a peroxide ligand bridging the two metals (*9*). The Fe_{a3}–O distance is significantly longer than that found in Fe^{3+}–OH^- compounds and is consistent with the high-spin heme a_3 present on the oxidized form (*10*). The O–O bond length (1.62 Å) is slightly longer than that of H_2O_2. One hydroxide ion and one water have been proposed for the ligands of the heme a_3–Cu_B site in the fully oxidized bacterial cytochrome c oxidase at 2.7 Å resolution (*8*). However, this model provides significantly higher residual density in an $(F_o - F_c)$ difference map than the peroxide model, that is, the bridging peroxide fits the electron density at 2.3 Å resolution significantly better than the hydroxide/water model.

The fully oxidized form given here is the enzyme preparation as purified from the tissue under aerobic conditions. In analogy to hemerythrin, in which the peroxide form is the stable oxygenated form (*11*), the bridging peroxide structure is consistent with the stability of the fully oxidized enzyme (*12*). The effect of x-ray irradiation under the present experimental conditions is negligible (*13*). The enzyme form is characterized by much slower reduction of heme a_3 (*14*) and much slower cyanide binding, compared with the enzyme under turnover conditions (*15*). Thus, the form may not directly participate in the catalytic turnover (*16*) and is called alternatively the resting oxidized form (*17*). The fully oxidized form directly involved in the catalytic turnover is called the oxygen pulsed form (*18*).

No ligand is detectable between Fe_{a3} and Cu_B in the multiple isomorphous replacement and density modification (MIR/DM) map and the $(F_o - F_c)$ difference map of the fully reduced form at 2.35 Å resolution (not shown). The three histidine imidazoles form a triangle with the Cu_B on the triangle plane. Such a Cu^{1+} coordination is usually very stable (*19*). Thus, the $Cu_B{}^{1+}$ is likely to be a poor ligand acceptor as well as a poor electron donor. This property may inhibit rapid formation of bridging O_2 between Fe_{a3} and Cu_B ($Fe_{a3}{}^{2+}$–O=O–$Cu_B{}^{1+}$), as has been proposed (*1*).

Inspection of interatomic contacts of the O_2 within the O_2 reduction site of the fully reduced enzyme shows that the hydroxyl group of Tyr^{244} is located close enough to form a hydrogen bond to the bound O_2 at $Fe_{a3}{}^{2+}$ (not shown). This hydrogen bond would stabilize the oxygenated form. Furthermore, Tyr^{244}, acidified by the covalent linkage to the imidazole nitrogen, donates, effectively, protons to the dioxygen reduction site through the hydrogen bond network connecting Tyr^{244} with the matrix

S. Yoshikawa, K. Shinzawa-Itoh, R. Nakashima, R. Yaono, and C. Peters Libeu are in the Department of Life Science, Himeji Institute of Technology and CREST, Japan Science and Technology Corporation (JST), Kamigohri Akoh, Hyogo 678–1297, Japan. E. Yamashita, N. Inoue, M. Yao, M. J. Fei, T. Mizushima, T. Tomizaki, and T. Tsukihara are at the Institute for Protein Research, Osaka University, 3-2 Yamada-oka, Suita 565–0871, Japan. H. Yamaguchi is at the Faculty of Science, Kwansei Gakuin University, Uegahara, Nishinomiya Hyogo 662, Japan.

*To whom correspondence should be addressed.

surface (*4*). The proximity of heme a to heme a_3, shown in the crystal structures of bovine heart and bacterial enzymes, suggests that heme a serves as an effective electron donor to heme a_3, consistent with a resonance Raman result (*20*) confirmed by the absorption spectral change (*21*). Thus, reduction of O_2 at heme a_3, which is hydrogen-bonded to Tyr^{244}, may be triggered by electron transfer from heme a to heme a_3 to produce a hydroperoxo adduct bound at $Fe_{a3}{}^{3+}$ (Fig. 1B).

After formation of the hydroperoxo species (Fig. 1B), the third electron from Cu_B, via His^{240}–Tyr^{244} linkage, and the second proton from the matrix side, via Tyr^{244}, may be donated effectively to the bound hydroperoxide to form a ferryloxo species (Fe^{4+}=O) and a water. However, the stable $Cu_B{}^{1+}$, as described above, may not donate the electron equivalent to the hydroperoxo adduct, but to Fe^{5+}=O formed after H_2O is released from the hydroperoxo adduct as suggested (*22*). In either mechanism, the life time of this hydroperoxo intermediate could be too short to detect consistently with the resonance Raman results (*22*). Ad-

Table 1. Intensity data and statistics of phase determination for the fully oxidized, fully reduced, fully reduced CO-bound, and fully oxidized azide-bound forms. Each structure was determined by multiple isomorphous replacement (MIR) (*37*).

	Native				Derivative		
	Oxidized form	Reduced form	CO form	Azide form	$IrCl_6$(I)	$IrCl_6$(II)	CH_3HgCl
Resolution (Å)*	100–2.3 (2.38–2.30)	100–2.35 (2.46–2.35)	100–2.8 (2.9–2.8)	100–2.9 (3.0–2.9)	100–3.0 (3.2–3.0)	100–3.0 (3.14–3.00)	100–3.0 (3.11–3.00)
Observed reflections	973,307 (90,077)	1,184,694 (55,541)	1,656,746 (49,385)	561,728 (30,449)	319,358 (18,599)	381,828 (28,410)	328,484 (15,186)
Independent reflections	284,634 (28,157)	270,061 (28,814)	173,384 (14,954)	133,932 (10,237)	125,036 (11,545)	133,245 (14,008)	127,548 (9,396)
$I/\sigma(I)$	30.9 (4.1)	14.4 (2.0)	14.7 (3.5)	10.0 (2.1)	10.0 (1.4)	21.3 (2.7)	12.4 (1.5)
Averaged redundancy†	3.3 (3.1)	4.4 (1.9)	9.5 (3.3)	4.2 (3.0)	2.6 (1.6)	2.9 (2.0)	2.6 (1.6)
Completeness‡	90.2 (89.9)	89.2 (72.0)	97.5 (85.0)	85.7 (66.3)	86.3 (64.5)	93.0 (79.1)	88.3 (65.7)
R_{merge}§	6.1 (25.1)	6.2 (32.0)	6.2 (32.0)	7.8 (31.7)	9.0 (29.6)	6.2 (23.4)	8.5 (28.4)
Oxidized form							
R_{iso}‖					0.220 (0.541)	0.167 (0.318)	0.256 (0.531)
R_{cullis}¶					0.85 (0.90)	0.87 (0.94)	0.90 (0.95)
Phasing power#					0.85 (0.57)	0.85 (0.62)	0.74 (0.44)
Reduced form							
R_{iso}‖					0.216 (0.439)	0.149 (0.249)	0.241 (0.448)
R_{cullis}¶					0.86 (0.96)	0.86 (0.95)	0.93 (0.96)
Phasing power#					0.89 (0.56)	0.81 (0.43)	0.69 (0.49)
CO form							
R_{iso}‖					0.192 (0.395)	0.144 (0.264)	0.237 (0.393)
R_{cullis}¶					0.92 (0.98)	0.85 (1.00)	0.85 (0.97)
Phasing power#					0.63 (0.26)	0.72 (0.32)	1.00 (0.43)
Azide form							
R_{iso}‖					0.118 (0.243)	0.154 (0.377)	0.205 (0.378)
R_{cullis}¶					0.92 (1.00)	0.92 (0.98)	0.85 (0.97)
Phasing power#					0.72 (0.32)	0.63 (0.26)	1.00 (0.43)

*Numbers in parentheses are given for the highest resolution shells. †Redundancy is the number of observed reflections for each independent reflection. ‡Completeness in a percentage of independent reflections observed. §R_{merge}: $\Sigma_h\Sigma_i|I(h,i)-\langle I(h)\rangle|/\Sigma_h\Sigma_i I(h,i)$, where $I(h,i)$ is the intensity value of the ith measurement of h and $\langle I(h)\rangle$ is the corresponding mean value of $I(h)$ for all i measurements; the summation is over the reflections with I/σ_I larger than 1.0. ‖R_{iso}: $\Sigma|F_{PH}-F_P|/\Sigma F_{PH}$, where F_{PH} and F_P are the derivative and the native structure factor amplitudes, respectively. ¶R_{Cullis}: $\Sigma||F_{PH}-F_P|-F_H(Calc)|/\Sigma|F_{PH}-F_P|$, where $F_H(Calc)$ is the calculated heavy-atom structure factor. The summation is over the centric reflections only. #Phasing power is rms isomorphous difference divided by rms residual lack of closure.

dition of another three equivalents of electrons and protons to the hydroperoxo species drives the catalytic process, including the oxygen pulsed state (*18*), to reproduce the original reduced species (Fig. 1B).

The fully oxidized resting form may be formed from the enzyme species with Tyr^{244} in the deprotonated state as described above. The deprotonated tyrosine cannot form a hydrogen bond to the bound O_2. In this case, the bound O_2 may form a bridging O_2 between Fe_{a3}^{2+} and Cu_B^{1+} to form Fe_{a3}^{3+}–O–O–Cu_B^{2+} (Fig. 1B) as the resting oxidized form. A possible physiological role of the fully oxidized resting form is to prevent the potentially very reactive O_2 reduction site from producing radical species with accidental contacts of O_2 to the site in the absence of sufficient amount of reducing equivalent in the enzyme molecule.

The distance between Fe_{a3} and Cu_B in the refined crystal structure is 4.9 Å in the fully oxidized state, 5.2 Å in the fully reduced state, 5.3 Å in the fully oxidized azide-bound state, and 5.3 Å in the fully reduced CO-bound state. These four crystal structures indicate that the position of Cu_B depends on either the oxidation state of the metal sites or ligand binding to Fe_{a3}, whereas Fe_{a3} is fixed. Fe_{a3}^{2+} in the fully reduced form without any ligand (in a five-coordinated ferrous high-spin state) is significantly closer to the porphyrin plane of heme a_3 than in the case of deoxy myoglobins (*23*).

CO coordinates to Fe_{a3} in a bent end-on manner (Fig. 2A and Table 3). The oxygen atom of CO is 2.5 Å away from Cu_B and forms a distorted trigonal pyramid with the three imidazole nitrogen atoms in the base and the oxygen at the apex. This long bond length as a coordination bond suggests a very weak interaction between Cu_B and the CO bound at Fe_{a3}, which is consistent with the infrared results (*24*). The refined structure of the azide-bound form at 2.9 Å resolution shows that azide forms a bridge between Fe_{a3} and Cu_B (Fig. 2B). One end of the azide and three histidine imidazoles provide a distorted square planar coordination to Cu_B in a manner similar to the peroxide binding in the fully oxidized form. The coordination structure of Cu_B, which includes three imidazole ligands, is in contrast to the reported structure of the azide-bound form of the bacterial enzyme in which one of the histidine imidazoles is missing (*3*).

Other metal sites. An electron density peak with a trigonal bipyramidal coordination that includes peptide carbonyls of Glu^{40}, Glu^{45}, and Ser^{441}, a water, and the side chain carboxyl of Glu^{40} (a counterion) is reasonably assigned to a Na^+ site (Fig. 2C). The thermal factor for the metal site as a Na^+ site supports this assignment (*25*). However, Ca^{2+} ion can be accommodated at the site by a small conformational change in the ligands nearby. This finding is consistent with the recent report for competition between Na^+ and Ca^{2+} for binding to a common site (*26*). The metal site is apparent in all the crystal structures presented here. A corresponding metal site in the bacterial cytochrome c oxidase involves two counter ion ligands out of five ligands (*8*). The structure difference between bovine and bacterial enzymes could induce the dependency of the Ca^{2+} effect on the biological species, recently reported (*26*).

The difference maps at 2.3 Å resolution show a structure of Mg^{2+} coordinated by Glu^{198} of subunit II, His^{368} and Asp^{369} of subunit I, and three water molecules (Fig. 2D). Two out of three water molecules were

Table 2. Statistics of structural refinements of oxidized, reduced, CO-bound, and azide-bound forms. Each structure was refined by simulated annealing followed by positional and *B* factor refinements with XPLOR (*6*).

State	Oxidized	Reduced	CO-bound	Azide-bound
Resolution (Å)	15.0–2.3	15.0–2.35	7.0–2.8	7.0–2.9
R*	0.220	0.211	0.213	0.193
R_{free}†	0.253	0.251	0.255	0.255
σ_{bond} (Å)	0.015	0.015	0.014	0.016
σ_{angle} (degrees)	2.1	2.1	2.1	2.1
rms‡ (Å)	0.30	0.30	0.32	0.33

*R is a conventional crystallographic R factor, $\Sigma||F_o| - |F_c||/\Sigma|F_o|$, where F_o and F_c are the observed and a calculated structure factor, respectively. †R_{free} is a free R factor of XPLOR refinement (*36*) evaluated for the 5% of reflections that are excluded from the refinement. ‡rms is a root mean square error of atomic coordinates estimated by the Luzatti plots (*38*).

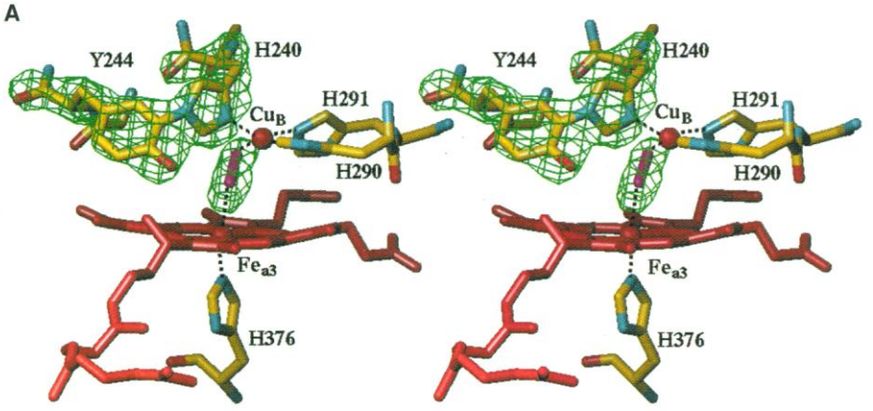

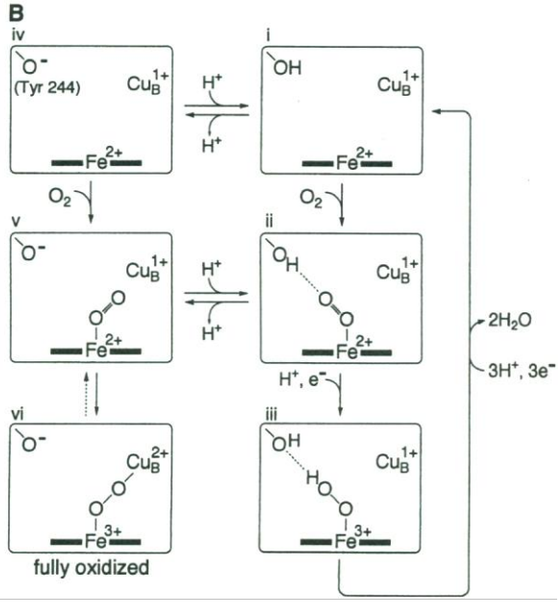

Fig. 1. Crystal structure of Fe_{a3}-Cu_B site of the fully oxidized form at 2.3 Å resolution and a possible role of Tyr^{244} in the mechanism of O_2 reduction. (**A**) The ($F_o - F_c$) difference Fourier map of the oxidized form calculated by omitting His^{240}, Tyr^{244}, and any ligand between Fe_{a3} and Cu_B from the F_c calculation. Contours are drawn at 7σ level (1σ = 0.0456 e^-/Å^3). (**B**) A possible mechanism for formations of the hydroperoxide intermediate and of the resting oxidized form. Protons (H^+) are from the hydrogen bond network and electrons (e^-) from heme a. Only the O_2 reduction site is shown. OH and O^- denote Tyr^{244} and its deprotonated form.

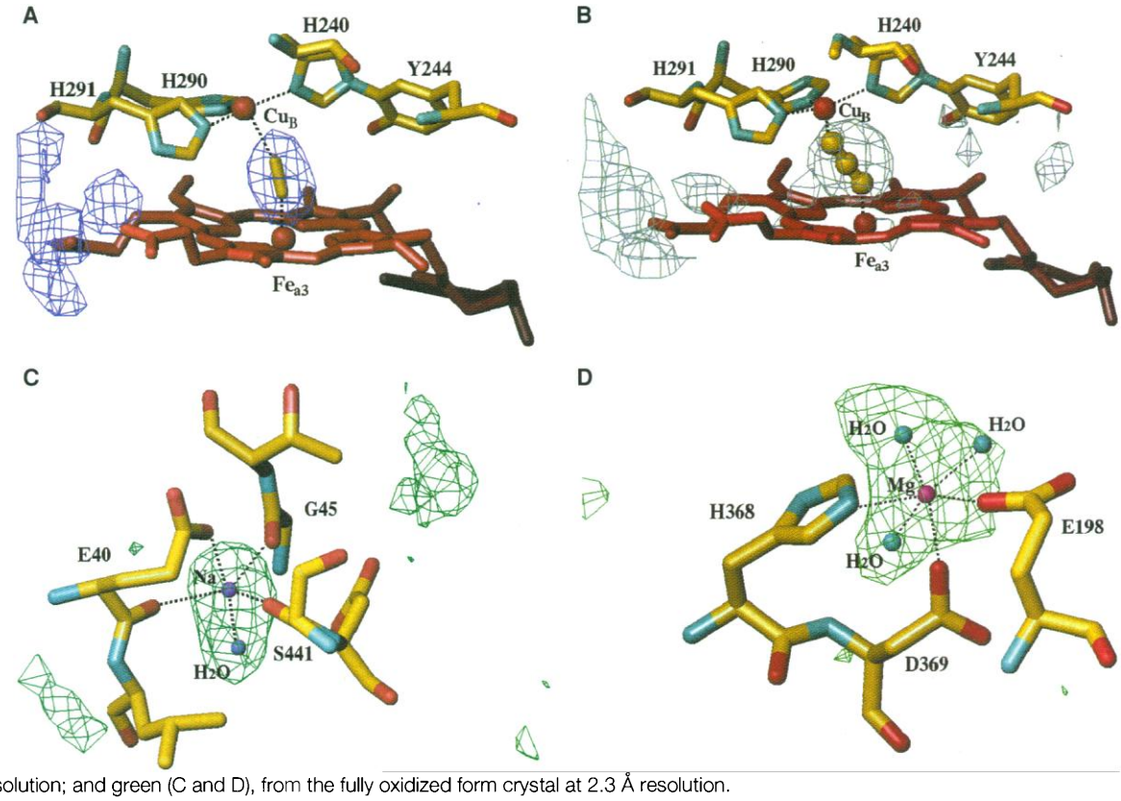

Fig. 2. Crystal structures of the Fe_{a3}–Cu_B site in the fully reduced CO-bound and fully oxidized azide-bound states and those of the Na^+/Ca^{2+} and Mg^{2+} sites. ($F_o - F_c$) difference Fourier maps for CO bound at Fe_{a3} at 3σ level (**A**) and azide bridging between Fe_{a3} and Cu_B at 2.2σ level (**B**) are given where the bound ligands and fixed waters are not included in the F_c calculation. The difference electron density maps at 4σ level (1σ = 0.0436$e^-/Å^3$) for the Na^+/Ca^{2+} site (**C**) and for the Mg^{2+} site (**D**). Violet, purple, and blue balls are the positions of Na^+, Mg^{2+}, and water, respectively. The colors of the electron densities denote the crystals from which the densities are obtained: purple (A), from CO derivative crystal at 2.8 Å resolution; cyan (B), from azide derivative crystal at 2.9 Å resolution; and green (C and D), from the fully oxidized form crystal at 2.3 Å resolution.

not shown in the crystal structures previously reported at 2.8 Å resolution (*2*).

Neither the ligand binding nor oxidation states induced any detectable conformational change in the Na^+/Ca^{2+} and Mg^{2+} sites.

Redox-coupled conformational change in the protein moiety. A segment from Gly^{49} to Asn^{55} moves toward the cytosolic surface by about 4.5 Å at the position of the carboxyl group of Asp^{51} on reduction of the fully oxidized enzyme (Fig. 3). One of the amino acid residues in the segment, Asp^{51}, in the fully oxidized state is completely buried inside the protein (Fig. 3). One of the oxygen atoms of the carboxyl group of Asp^{51}, which is completely buried inside the protein in the fully oxidized state and does not contribute to the accessible surface calculated with a 1.4 Å probe, contributes to the accessible surface in the fully reduced state (Fig. 3) (*27*). No other significant conformational change is detectable in the electron density distribution of the protein moiety.

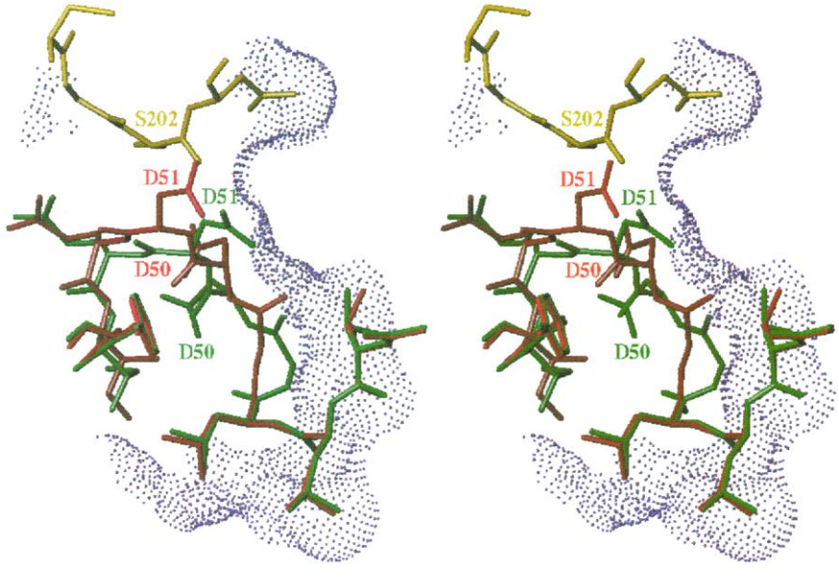

Fig. 3. Redox-coupled conformational change in the segment from Gly^{49} to Asn^{55}. The conformation of the segment in the fully oxidized form is stereoscopically shown in red, and that in the fully reduced form in green. The yellow structure denotes subunit II with no redox-coupled conformational change. The accessible surface for the fully oxidized state (*35*) is indicated by dots.

Asp^{51}, in the fully oxidized state, is connected with the matrix surface by a network that includes a peptide unit, hydrogen bonds, a cavity, and a water path (Fig. 4A). The peptide bond connecting Asp^{51} and Tyr^{54} with hydrogen bonds on both ends can act as a unidirectional proton transfer path from Tyr^{54} to Asp^{51}, because it is in an equilibrium state between the two tautomers, –CO–NH– and –C(OH)=N–, where the former is much more abundant than the latter. Tyr^{54}, a propionate group of heme a, Tyr^{371}, a fixed water, and Arg^{38} are connected by hydrogen bonds. Arg^{38} is on the boundary of a large cavity that lacks any detectable electron density but is large enough to contain randomly oriented or mobile water molecules. The cavity is connected with the matrix surface by a water path, which includes some hydrophilic ami-

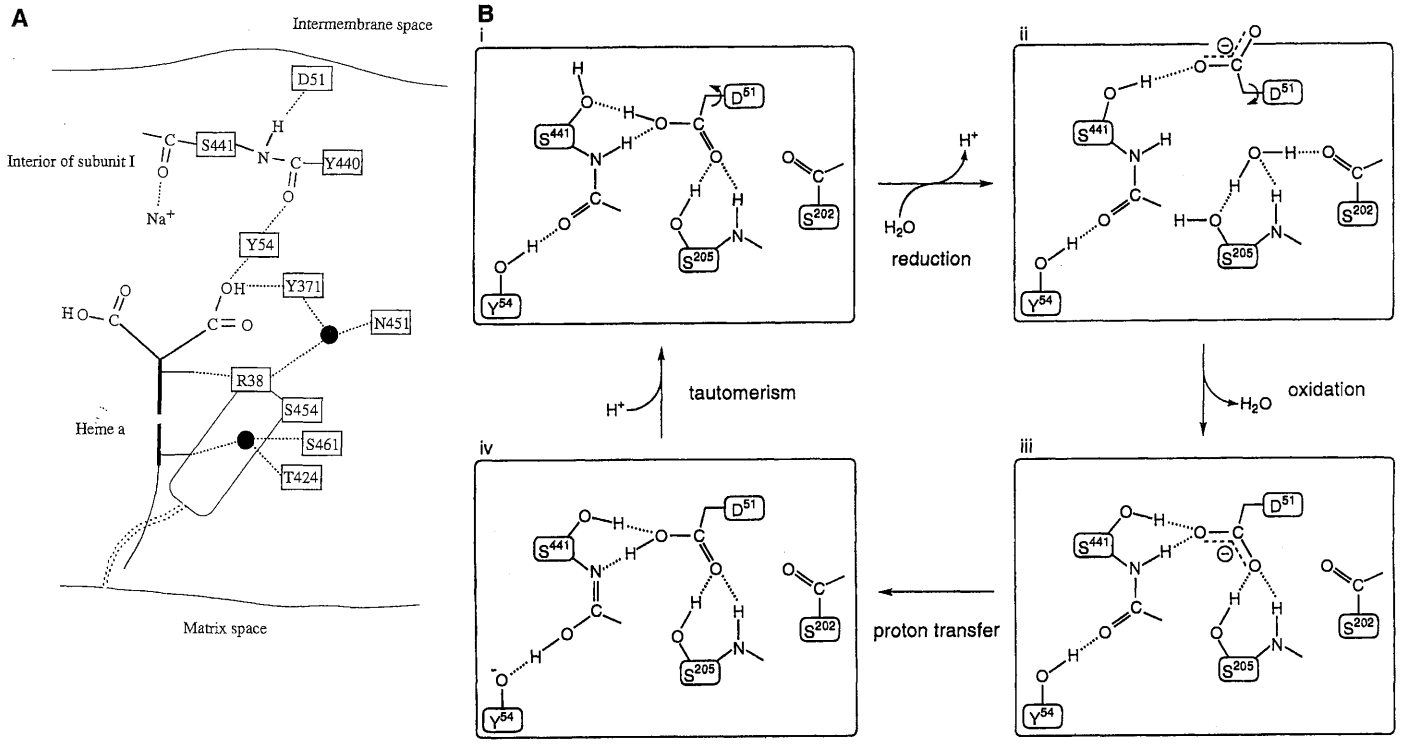

Fig. 4. Schematic representations of the structure of the proton pumping system and a possible function of Asp^{51} in the proton pumping by cytochrome c oxidase. (**A**) The hydrogen bond network from Asp^{51} to the matrix surface. Dotted lines denote hydrogen bonds. The small, dark circles indicate fixed waters. A thick stick denotes a side view of the porphyrin plane of heme a, and thin sticks (from top to bottom) are the side chains, propionates, formyl, and hydroxyl farnesylethyl. The hydroxyl farnesylethyl group is in the water path with its hydroxyl group hydrogen bonded to Ser^{461} and Thr^{424} via a water fixed on the boundary of the cavity. The porphyrin plane is a part of the boundary of the cavity. The formyl group is hydrogen-bonded to Arg^{38}, and one of the propionate groups is hydrogen-bonded to Tyr^{371} and Tyr^{54}. The Na^+ site is also shown. (**B**) A possible mechanism for a unidirectional proton transfer by Asp^{51}. Dotted lines denote hydrogen bonds. Direction of the movement of Asp^{51} side chain is shown by arrows. Deprotonated carboxyl groups are shown by broken lines.

no acid side chains of helices XI and XII of subunit I (*4*) and the hydrophobic farnesyl group of heme a. The diameter of the tube at the narrowest point is approximately three-quarters the size of water. However, molecular dynamics calculations have shown that small molecules can travel through spaces much smaller than their row radii in static models (*28*). Thus, Asp^{51} in the fully oxidized state can take up protons only from the matrix side but is inaccessible to the cytosolic side. The above hydrogen bond network was not described in (*2*), because Asp^{51} at the cytosolic end of the network is inaccessible to the bulk water without movement of the peptide backbone (*29*). This network interacts with heme a at several points (Fig. 4A), suggesting a function of the network under redox control.

On reduction of this enzyme, the hydrogen bond between the peptide amide of Ser^{441} and the carboxyl group of Asp^{51} is broken, and Asp^{51} loses its accessibility to the matrix side through the hydrogen bond network. The conformation of the segment from Gly^{49} to Asn^{55} seems to be determined only by the oxidation state of the metal sites, because the fully oxidized azide-bound form shows the conformation identical to that of the fully oxidized form, and the fully reduced CO-bound form provides the conformation of the fully reduced form. These properties strongly suggest that Cu_B does not control the conformation of Asp^{51} and that the conformation of the Asp^{51} segment of the resting oxidized form, which is not involved in the catalytic turnover (*16*, *17*), is identical to that of the oxygen pulsed state, which is active under turnover conditions (*18*).

The above results suggest the following redox-coupled proton pumping mechanism (Fig. 4B). Asp^{51}, in the fully oxidized state, is hydrogen-bonded with Ser^{205} of subunit II and Ser^{441} of subunit I each at both its hydroxyl group and its peptide amide. The protonated carboxyl group (–COOH) of Asp^{51} in the fully oxidized state become accessible to the bulk water to release protons on reduction. Meanwhile, the carboxyl group breaks three hydrogen bonds out of four, leaving the one to the hydroxyl of Ser^{441}. A water molecule is fixed with hydrogen bonds to Ser^{205} at both its hydroxyl and peptide amide and to the peptide carbonyl of Ser^{202}. On reoxidation of the enzyme, the fixed water is replaced by the

Table 3. Structures of the O_2 reduction site in four different states. Positional and *B*-factor refinement was applied for each structure determination of O_2 reduction site with the program XPLOR (*6*, *39*).

State	Bridging ligand	Distance (Å)*		
		Fe_{a3}-Cu_B	Fe_{a3}-X†	Cu_B-Y‡
[Fe_{a3}^{3+}, Cu_B^{2+}]				
Fully oxidized	O_2^{2-}	4.91	2.52	2.16
Azide bound	N_3^-	5.30	1.97	1.90
[Fe_{a3}^{2+}, Cu_B^{+}]				
Fully reduced		5.19		
CO bound	CO	5.27	1.90	2.47

*Averaged distances of two independent molecules in the crystal are given. †A short interatomic distance between Fe_{a3} and a ligand atom and ‡that between Cu_B and another ligand atom.

deprotonated carboxyl group ($-COO^-$) of Asp^{51}. The $-COO^-$ extracts a proton of the peptide amide and creates a deprotonated peptide. The peptide is reprotonated readily by Tyr^{54}, which is hydrogen bonded to the carbonyl group of the peptide providing the –C(OH)=N–form. Transition to the stable tautomer of the peptide and reprotonation of Tyr^{54} by means of a proton from the matrix side give the original structure of the fully oxidized state (Fig. 4B).

The redox transition of heme a, which interacts with the hydrogen bond network between Asp^{51} and the matrix surface as described above, is likely to contribute to driving the active transport of protons. The mechanism by which protons are released on oxidation of the enzyme, in contrast to the one presented in Fig. 4B, is also possible (*30*), consistent with biochemical results (*31*).

The present results suggest a proton pumping site apart from the heme a_3–Cu_B site, in contrast to the direct coupling mechanism for the proton pumping in which one of the histidines liganded to Cu_B serves as a proton carrier (*32*). The latter mechanism is supported by the crystal structure of the azide-inhibited bacterial enzyme that lacks the electron density of one of the histidines coordinated to Cu_B (*3*). Iwata and colleagues proposed a possible proton transfer path to the proton pumping site, His^{290} (in the numbering of bovine heart enzyme), from Asp^{91} via Glu^{242} (*3*). On the other hand, the crystal structure of bovine heart enzyme shows the electron density distribution for His^{290} even in the azide-bound fully oxidized form as described above. In any forms of bovine heart enzyme, the hydrogen bond network from Asp^{91} ends at Glu^{242}. No possible proton transfer path is detectable from Glu^{242} to His^{290} in the crystal structures of bovine heart enzyme. Furthermore, no fixed water connecting the two amino acids is detectable even in the crystal structures of bovine heart cytochrome c oxidase at 2.30 to 2.35 Å resolution. Thus, any crystal structure of bovine heart cytochrome c oxidase available at present does not support the proposal (*33*) for the proton transfer from Glu^{242} to His^{290} or to His^{291}.

Glu^{242} is hydrogen bonded to the sulfur atoms of Met^{71}, Sγ-O distance of 3.2 Å, in any crystal structure given here, indicating that the carbonyl group is in COOH form, regardless of the oxidation and ligand-binding states, which is consistent with the recent infrared investigation (*33*).

If the proton pumping pathway includes the O_2 reduction site (the heme a_3–Cu_B site), protons to be pumped must be sorted effectively from those for making water as suggested (*32*, *34*). Otherwise, the protons to be pumped are used for making H_2O at the O_2 reduction site. However, the crystal structure of bovine enzyme shows no structure suggesting such a function.

All the amino acids in the network connected to Asp^{51} in bovine heart enzyme are conserved in animals from human to sea urchin. However, Asp^{51} and Tyr^{54} are not conserved in plant and bacterial enzymes. These differences suggest an evolution in the proton pumping pathway.

REFERENCES AND NOTES

1. B. G. Malmström, *Chem. Rev.* **90**, 1247 (1990); S. Ferguson-Miller and G. T. Babcock, *ibid.* **96**, 2889 (1996).
2. T. Tsukihara *et al.*, *Science* **269**, 1069 (1995).
3. S. Iwata, C. Ostermeier, B. Ludwig, H. Michel, *Nature* **376**, 660 (1995).
4. T. Tsukihara *et al.*, *Science* **272**, 1136 (1996).
5. Purification of the enzyme preparation with repeated recrystallization is the most critical for improvement of the crystallization conditions of this enzyme. The crystals of fully reduced and CO-bound fully reduced forms were prepared by soaking the crystals of fully oxidized form in the medium containing ascorbate and a catalytic amount of cytochrome c as a reducing system and polyethylene glycol (PEG 4000) for stabilizing crystals under N_2 and CO atmosphere, respectively. X-ray diffraction experiments were performed on these forms by placing crystals in capillaries filled with the appropriate soaking media. The oxidation state and the ligand-binding state of the enzyme were confirmed by absorption spectra of these crystals taken under the same medium conditions. Azide form was prepared by soaking the crystals of fully oxidized form into the buffer containing azide and appropriate amount of PEG 4000 under aerobic conditions. Intensity data were collected with synchrotron radiation of 1.0 Å at the Photon Factory, Tsukuba, Japan, by means of a modified Weissenberg camera for macromolecules [N. Sakabe, *J. Appl. Crystallogr.* **16**, 542 (1983)].
6. A. Brunger, J. Kuriyanan, M. Karplus, *Science* **235**, 458 (1987).
7. $(F_o - F_c)$ difference electron density map is calculated with coefficients of $(F_o - F_c)\exp(i\alpha_c)$, where F and α are the structure factor and phase angle, respectively, and suffixes o and c represent the observed and calculated value, respectively.
8. C. Ostermeier, A. Harrenga, U. Ermler, H. Michel, *Proc. Natl. Acad. Sci. U.S.A.* **94**, 10547 (1997).
9. The residual electron density between Fe_{a3} and Cu_B is consistent also with a hydroperoxo ligand bound at Cu_B (Cu_B-O-O-H) in which the oxygen atom not directly bound to Cu_B coordinates to Fe_{a3}^{3+}, as follows:

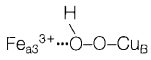

10. B. F. Van Gelder and H. Beinert, *Biochem. Biophys. Acta* **189**, 1 (1969).
11. M. A. Holmes, I. Le Trong, S. Turley, L. C.Sieker, R. E. Stenkamp, *J. Mol. Biol.* **218**, 583 (1991).
12. Six electron equivalents are required for complete reduction of the fully oxidized form, which contains a bridging peroxide. The stoichiometry is inconsistent with the reported value, four equivalents [(*7*); G. C. M. Steffens, T. Soulimane, G. Wolfe, G. Buse, *Eur. J. Biochem.* **213**, 1149 (1993)]. However, higher experimental accuracy for the redox titration is required for distinction between four and six electron equivalents. Furthermore, the molecular extinction coefficient of the absorption spectrum of the enzyme usually based on the iron content must be determined accurately for the stoichiometry determination. Contaminant irons that can be removed only by crystallization were found in the enzyme preparation. The fully oxidized form can be kept at 4°C in the crystalline state for 8 months or longer without any significant change in the absorption spectrum or the enzymatic activity. (S. Yoshikawa, unpublished data).
13. The peroxo bridge in the above electron density map of the enzyme crystals at 8°C is also found in the crystal structure of the enzyme at liquid nitrogen temperature, at 2.4 Å resolution. Furthermore, no significant modification by x-ray irradiation under the present experimental conditions was detectable in the absorption spectrum and the enzymic activity of the enzyme in the crystalline state. These results indicate that the peroxide structure is not produced by x-ray irradiation. The negligible effect of x-ray exposure is likely caused by the short wavelength (1.0 Å) of the x-rays used here.
14. Q. H. Gibson, C. Greenwood, D. C. Wharton, G. Palmer, *J. Biol. Chem.* **240**, 888 (1965).
15. G. M. Baker, M. Noguchi, G. Palmer, *ibid.* **262**, 595 (1987).
16. M. T. Wilson *et al.*, *Proc. Natl. Acad. Sci. U.S.A.* **78**, 7115 (1981).
17. G. W. Brudwig, T. H. Stevens, R. Morse, S. I. Chan, *Biochemistry* **20**, 3912 (1981).
18. E. Antonini, M. Brunori, A. Colosimo, C. Greenwood, M. T. Wilson, *Proc. Natl. Acad. Sci. U.S.A.* **74**, 3128 (1977).
19. F. A. Cotton and G. Wilkins, *Advanced Inorganic Chemistry: A Comprehensive Text* (Wiley-Interscience, New York, ed. 4, 1980).
20. S. Han, Y. Ching, D. L. Rousseau, *Proc. Natl. Acad. Sci. U.S.A.* **87**, 8408 (1990).
21. M. I. Verkhovsky, J. E. Morgan, M. Wikström, *Biochemistry* **33**, 3079 (1994).
22. T. Kitagawa and T. Ogura, *Prog. Inorg. Chem.* **45**, 431 (1997).
23. In the fully reduced state, Fe_{a3} atom is displaced 0.12 Å from the plane formed by four pyrrole nitrogen atoms toward histidine coordinated to Fe_{a3}. The distance between Fe_{a3} atom in the fully oxidized state and the pyrrole nitrogen plane is 0.07 Å. In contrast, the distances for deoxy and metmyoglobins are 0.3 and 0.09 Å, respectively [M. L. Quillin, R. A. Arduini, J. S. Olson, G. N. Phillips Jr., *J. Mol. Biol.* **234**, 140 (1993)].
24. S. Yoshikawa and W. S. Caughey, *J. Biol. Chem.* **257**, 412 (1982).
25. The thermal factor calculated with Na^+ ion for the electron density peak is almost identical with those of the ligand atoms, whereas a 10 to 15 $Å^2$ higher thermal factor relative to those of ligand atoms is obtained when Ca^{2+} ion is used. The trigonal bipyramidal configuration suggests Na^+ rather than Ca^{2+} as the metal ion. The number of counter-ion in the ligands, only carboxyl group of Glu^{40}, is also consistent with Na^+ ion.
26. A. Kirichenko, T. V. Vygodina, H. M. Mkrtchyan, A. A. Konstantinov, *FEBS Lett.* **423**, 329 (1998).
27. When Gly-Asp-Gly is used as the standard for 100% accessibility, Asp^{51} has an accessibility of 12% in the fully reduced state and 0% in the fully oxidized state (*35*). This significant increase in accessibility from 0% upon reduction should be accompanied by a significant decrease in pK of the carboxyl group of Asp^{51}.
28. D. A. Case and M. Carplus, *J. Mol. Biol.* **132**, 343 (1979).
29. The bottom half of the network (that is, the cavity and the water path) is common to one of the proton channels shown in figure 10B of (*4*) where Arg^{38} is connected with Asp^{407} at the matrix surface by hydrogen bonds and small cavities (*2*). However, further refinement of the structure along the network reveals a water path that includes the hydrogen bond network. The other hydrogen bond network, a possible proton pumping path, which includes Asp^{91} near the matrix end and Ser^{142} on the cytosolic end (*4*), does not show any redox-coupled conformational change. Thus, regardless of the oxidation and ligand-binding states, the hydrogen bond network is disconnected at two points between Asn^{98} and Ser^{156} and between Ser^{115} and Ser^{142}, as described (*4*). However, we cannot exclude the possibility that the hydrogen bond network functions as a proton pumping site, because a conformational change, without any movement of peptide back bones, that forms a new hydrogen

bond at the disconnected points may occur only within limited time, too short to be detected in the crystal structure.
30. If the carbonyl group of Asp^{51} in the deprotonated state is moved toward the cytosolic side on reduction, thereby leaving the proton on the H_2O hydrogen-bonded to Ser^{205} of subunit II, then the proton on the H_2O is pumped out as a hydronium ion on oxidation of the enzyme. The hydrogen-bond structure of the water fixed on Ser^{202} and Ser^{205} allows the fixed water to hold a proton.
31. N. Capitano *et al.*, *Biochim. Biophys. Acta* **1318**, 255 (1997).
32. M. Wikström *et al.*, *ibid.* **1187**, 106 (1996).
33. S. Riistama *et al.*, *FEBS Lett.* **414**, 275 (1996); A. Puustinen *et al.*, *Biochemistry* **36**, 13195 (1997).
34. R. J. P.Williams, *Nature* **376**, 643 (1995).
35. Calculated with program SURFACE of CCP4 package [B. Lee and F. M. Richards, *J. Mol. Biol.* **55**, 379 (1971); A. Shrake and J. A. Rupley, *ibid.* **79**, 351 (1973)].
36. A. T. Brunger, *Nature*, **355**, 472 (1992).
37. The derivative data sets used for the present structure analyses were the same as those for the previous structure analysis of the oxidized form at 2.8 Å resolution (*2*, *4*). Initial phases of each crystalline state were determined by MIR at 3.0 Å resolution with the program MLPHARE [Z. Otowinowski, MLPHARE (Collaborative Computational Project 4, Daresbury Laboratory, Warrington, UK, 1991), p. 80]. The initial MIR phases were extended from 5 Å to the highest resolution of each crystal in 200 small steps by DM consisting of solvent flattening [B. C. Wang, *Methods Enzymol.* **115**, 90 (1985)], histogram matching [K. Y. J. Zhang and P. Main, *Acta Crystallogr.* **A46**, 377 (1990)], and noncrystallographic symmetry averaging [M. Buehner *et al.*, *J. Mol. Biol.* **82**, 563 (1974); P. Argos *et al.*, *Acta Crystallogr.* **B32**, 2975 (1975)]. The phase extensions were carried out with the program DM of CCP4 (Collaborative Computational Project 4, 1994). Phases obtained by the density modification were combined with the initial phases determined by MIR. A free *R* factor of DM (*36*) for 5% of reflections in each shell and a correlation coefficient between electron density distributions of two independent molecules, $\{\Sigma\langle\rho_1 - \langle\rho_1\rangle\rangle\langle\rho_2 - \langle\rho_2\rangle\rangle/\Sigma[\langle\rho_1 - \langle\rho_1\rangle\rangle^2\langle\rho_2 - \langle\rho_2\rangle\rangle^2]^{1/2}\}$, were calculated at each stage of the density modification to monitor progress of the refinement. After the refinement of the phases by the density modification, the respective free *R* factors of DM and correlation coefficients converged to 0.279 and 0.907 for the oxidized form, 0.266 and 0.906 for the reduced form, 0.279 and 0.905 for the CO form, and 0.271 and 0.879 for the azide form. Coordinates have been deposited in the Protein Data Bank.
38. V. Luzzati, *Acta Crystallogr.* **5**, 802 (1952).
39. The structure determination of the heme a_3–Cu_B site in the oxidized form was carried out at 2.3 Å resolution under nine different restraint conditions for the O-O bond distances of 1.3, 1.4, 1.5, 1.6, 1.8, 2.0, 2.2, 2.5, and 2.8 Å, without any restraint for distances of Fe_{a3}–O and Cu_B–O. The refinement with 1.6 Å O-O distance restraint resulted in the smallest residual density at the O_2 reduction site in the $(F_o - F_c)$ difference map. In the structure determination of the azide form at 2.9 Å resolution, the distance between the Fe_{a3} and a nitrogen atom at one end of the azide molecule, and the distance between Cu_B and a nitrogen at the other end, were restrained to 2.07 and 1.90 Å, respectively, according to the analogous distances in the azide-bound structure of myoglobin [A. Mattevi *et al.*, *J. Mol. Recognition* **4**, 1 (1991)] and in ascorbate oxidase [A. Messerschmidt, H. Luecke, R. Huber, *J. Mol. Biol.* **230**, 997 (1993)]. The azide molecule was constrained to a linear rigid conformation. The reduced form was refined at 2.35 Å resolution without any ligand group between the dinuclear metal sites. The restraints used for the CO form were a C-O distance of 1.20 Å, an Fe_{a3}-C distance of 1.78 Å, and a perpendicular orientation of the Fe_{a3}–C to the heme plane in analogy to the CO form of a hemoglobin [G. E. O. Borgstrom, P. H. Roger, A. Arnone, *J. Mol. Biol.* **236**, 817 (1994)]. The structure of the heme a_3–Cu_B site of each crystal has been verified by the $(F_o - F_c)$ difference map.
40. We thank N. Sakabe and N. Watanabe for data collection with the Weissenberg camera and synchrotron radiation. Supported in part by Grants-in-Aid for Scientific Research on Priority Area (Molecular Science on the Specific Roles of Metal Ions in Biological Functions to S.Y.), and Grants-in-Aid for Scientific Research (grant 40068119 to S.Y. and 06558102, 06276102, and 05244102 to T. Tsukihara) from the Ministry of Education and Culture of Japan, and Grant-in-Aid for "Research for the Future" Program from the Japan Society for the Promotion of Science (JSPS-RFTF96L00503 to T. Tsukihara). This research was done with the approval of the Photon Factory Advisory Committee, and the National Laboratory for High Energy Physics, Japan (Proposal 91-050 and 94G-041). T. Tsukihara and S.Y. are members of the TARA project of Tsukuba University and senior visiting scientists of RIKEN.

2 January 1998; accepted 23 April 1998